Journal of Alloys and Compounds 849 (2020) 156384

Contents lists available at ScienceDirect

Journal of Alloys and Compounds

journal homepage: http://www.elsevier.com/locate/jalcom

Unit cell volume reduction of Gd5(Si,Ge)4 nanoparticles controlled by bulk compressibility

V.M. Andrade [a, b, *], J.H. Belo [a], N.R. Checca [c], A. Rossi [c], F. Garcia [c], B. Almeida [e], J.C.G. Tedesco [g], A. Poulain [f], A.M. Pereira [a], M.S. Reis [d], J.P. Araújo [a]

[a] IFIMUP, Physics Department of Science Faculty, Porto University, Porto, Portugal
[b] Gleb Wataghin Physics Institute, State University of Campinas (IFGW-UNICAMP), Campinas SP, Brazil
[c] Brazilian Center for Research in Physics - CBPF, Rio de Janeiro, Brazil
[d] Institute of Physics, Fluminense Federal University, Niteroi-RJ, Brazil
[e] CF-UM-UP, Department of Physics, University of Minho, Gualtar Campus, Braga, Portugal
[f] European Synchrotron Radiation Facility, Grenoble, France
[g] Polytechnic Institute, Rio de Janeiro State University, Nova Friburgo, RJ, Brazil

ARTICLE INFO

Article history:
Received 4 May 2020
Received in revised form
9 July 2020
Accepted 12 July 2020
Available online 10 August 2020

Keywords:
Rietveld refinement
Structural characterization
Nanostructures
Pulsed laser deposition

ABSTRACT

The production of $Gd_5(Si,Ge)_4$ compounds in reduced dimensionality, through pulsed laser deposition (PLD), have shown their potential for practical applications. Here, we present nanoparticles ranging from 10 to 27 nm of average particle size of $Gd_5(Si_xGe_{1-x})_4$, with x = 0, 0.45 and 0.60, obtained using an Nd:Yag (1064 nm) and an Excimer KrF laser (248 nm). Synchrotron X-ray Diffraction measurements revealed a reduced unit cell volume in comparison to their bulk counterpart. The x = 0 sample presented a ~1.99% reduction while x = 0.45 composition, a shrinkage of ~1.81% on the unit cell volume that are a result of a structural change to a Gd_5Si_4-type structure [O(I)]. In contrast, x = 0.60 nanoparticles conserve the bulk crystal structure with ~ 0.95% of volume shrinkage. As a consequence, there is a change on the magnetic transition order from a first to a second one for all nanostructures followed by a magnetocaloric response reduction. These observations unveil a direct correlation between the bulk compressibility values and the unit cell shrinkage, suggesting that the rise of a surface stress plays a major role on the particle and unit cell dimensions.

1. Introduction

Materials with multiple ferroic orderings are fundamentally interesting due to their rich and complex physics being technologically promising candidates for a wide range of applications, such as energy harvesting, refrigeration, sensors/actuators, biomedical, among others [1,2]. The important properties of these multiferroic systems rise from their strong coupling between structure and magnetic/electronic features. Reducing these systems to the micro/nanometric scales can give rise to novel properties related to intrinsic and extrinsic mechanisms like a negative thermal expansion [3] and magnetoelectric coupling [4], respectively. Although there is an advantage of innovative appliances emerging from the reduction of scale in these systems, controlling their intrinsic features is of great matter for the optimization of their production on a large scale [5]. For instance, it is known that most of the pure metallic materials present a reduction of the lattice parameters at the nanometric particle size and, consequently, the unit cell volume [6]. This shrinkage is due to the appearance of a negative surface tension associated with the surface/volume ratio increase leading to an intrinsic pressure in nanostructures. Several studies and theoretical models revealed that this mechanism is closely related to the bulk properties, more specifically, the volumetric compressibility [7,8].

Among the most known systems presenting a strong magneto-volume coupling, it is possible to mention the $La(Fe,Si)_{13}$ compounds, Heusler alloys [9] and the $Gd_5(Si,Ge)_4$ family compounds [10]. The latter one, which is the focus of the present study, was the responsible for the revival of the magnetic refrigeration at room temperature in 1997 when Pecharsky and Gschneidner discovered the giant Magnetocaloric Effect (MCE) in the $Gd_5Si_2Ge_2$

* Corresponding author. FIMUP, Physics Department of Science Faculty, Porto University, Porto, Portugal.
E-mail addresses: vandrade@ifi.unicamp.br, viviancamposandrade@gmail.com (V.M. Andrade).

https://doi.org/10.1016/j.jallcom.2020.156384
0925-8388/

composition [11]. A limited number of studies on the $Gd_5(Si,Ge)_4$ family at low dimensionality can be found up to date. The main experimental issues concerning the accomplishment of micro/nanostructures of these compounds rely on phase stabilization and oxidation [12]. The first attempts to produce nanometric samples is possible to mention the RF magnetron sputtering [13] and ball milling [14] techniques, where the formation of oxides and secondary phases could not be avoided. Currently, the successful examples of the production of $Gd_5(Si,Ge)_4$ nanostructures comprise the use of pulsed laser ablation techniques. Hadimani et al. were the first to demonstrate that the femtosecond pulsed laser deposition (PLD) technique using a bulk sample as the target allows the production of $Gd_5Si_2Ge_2$ granular thin films with ~600 nm of thickness [15]. Magnetic and structural characterization revealed that only ~10% of the sample volume presented the desired phase after the ablation with an ~800 nm wavelength laser. More recently, a $Gd_5Si_{1.3}Ge_{2.7}$ granular film with a thickness of ~790 nm and ~80 nm of particle size was achieved using a fs PLD [16] displaying a magnetostructural transition and, consequently, a large magnetocaloric effect, despite the presence of a small fraction of non-$Gd_5(Si,Ge)_4$ phases. These examples soundly demonstrate the potential of using femtosecond lasers where the particle formation occurs by an instantaneous fragmentation of the target material out of the thermodynamic equilibrium conditions. However, the use of a more conventional technique should be a pursuit to obtain nanostructured $Gd_5(Si,Ge)_4$ samples aiming for practical applications [17].

As an alternative, a more accessible laser with a nanosecond pulse duration can be a path to optimize the production of these nanostructures. For instance, Tarasenka et al. were able to produce $Gd_5Si_2Ge_2$ nanoparticles through pulsed laser ablation in liquids (PLAL) using an Nd:Yag laser with pulse durations of 8 ns [18]. The authors ablated the starting reactants in separate cells filled with ethanol. The colloidal solutions were then mixed for a subsequent ablation in a double-pulse configuration. From this procedure, nanostructures with particle size ranging between 30 and 60 nm were achieved. The structural characterization revealed the formation of $Gd_5Si_2Ge_2$ phase together with other undesired phases. It is worth noting that the $Gd_5Si_2Ge_2$-type monoclinic structure formation remains a challenging task even for bulk samples [19]. A recent study of Tarasenka et al. regarding Gd-Si-Ge colloidal solutions production through the PLAL method showed that the temperature increase is the primary mechanism of particle growth during ablation that leads to co-melting and chemical interactions [20]. However, reasonable control of the final sample composition also depends on the laser fluence, when the separated Gd, Si and Ge colloidal solutions are ablated together. Besides the requirement of good local temperature control due to the changes in their melting points. These observations reveal that nanosecond pulsed lasers can also be used to produce $Gd_5(Si,Ge)_4$ crystal structures at the nanometric scale. The particle formation process from ablations in liquids presents a more complex thermodynamic mechanism where spallation, Coulomb explosion and spinodal decomposition occur in addition to further laser interactions with the ejected material [21]. In this regard, an approach to make the $Gd_5(Si,Ge)_4$ nanostructures fabrication process more accessible can be achieved by using a ns pulsed laser using inert gases. Indeed, the nanosecond ablation in the presence of inert gas is within the classical regime of beam-matter interactions where the particle formation is given by atomic nucleation followed by successive collisions that lead to coalescence and agglomeration [22].

For the reasons here stated, an Nd:YAG laser (1064 nm) was chosen to produce $Gd_5(Si_xGe_{1-x})_4$ nanoparticles with $x = 0$ and a KrF Excimer laser (248 nm) for the synthesis of $x = 0.45$ and 0.60 compositions, using Ar gas as an inert medium for particle growth during the ablation. Once the increase of Si content changes the structure type for the $Gd_5(Si,Ge)_4$ compounds, the stoichiometries were selected to cover all the possible adopted structures: orthorhombic-II [O(II)] for $x = 0$; monoclinic for $x = 0.45$ and; orthorhombic-I [O(I)] for $x = 0.60$ composition. To produce the NPs, the bulk alloys with the chosen stoichiometries were used as the targets to guarantee the correct compositions. The KrF Excimer laser wavelength presents a higher penetration depth, while the laser wavelength closer to UV is an advantage for metals ablation since reflectance decreases in the UV region, improving the ablation rate during synthesis [23,24]. Also, the selected stoichiometries $x = 0.45$ and 0.60 are in the limit of a phase mixed region to demonstrate the feasibility of this technique along with the family phase diagram. From this process, nanoparticles with 10–27 nm were obtained with good crystalline features and with no significant secondary phases fractions, as confirmed by magnetic, structural and morphological analysis. In particular, for $x = 0.45$ composition, there is a change in symmetry from a monoclinic of the bulk to an orthorhombic-I structure for the nanostructures that lead to a unit cell volume shrinkage. A linear trend is found between the bulk compressibility and unit cell volume reduction with the Si content (x) in the samples prepared by femtosecond from Ref. [3] and nanosecond PLD techniques, revealing that the mechanism of particle formation is associated with the intrinsic features of the ablated bulk target.

2. Materials and methods

Targets synthesis: Bulk samples of $Gd_5(Si_xGe_{1-x})_4$ with $x = 0.00$, 0.45 and 0.60 obtained by Tri-arc melting the starting metals with purity higher than 99.99% weighted to obtain the correct stoichiometries. The structural analysis of the bulk was performed through *Rietveld* refinement of the XRD patterns to guarantee a good quality of the nanoparticles. Afterwards, these ingots were cleaned, polished, and put into a stainless steel support rotating at 1 RPM to be used as the target for the ablation.

Nanoparticles synthesis: Before the deposition, due to Gd^{3+} reactivity with oxygen, the chamber was pumped by a turbomolecular pump for 2 h and Ar purged in order to remove the remnant O_2. The ingots were ablated, at room temperature, by an Excimer KrF laser with 248 nm of wavelength, pulse duration of 25 ns with a repetition of 10 Hz and a maximum energy of 550 mJ at Minho University. As for $x = 0$ composition, an Nd:YAG laser with 1064 nm of wavelength was used to ablate the target with a maximum energy of 200 mJ and pulse duration of 20 ns at the Physics Institute of Fluminense Federal University. In both depositions, the target surface was clean by ablating it with low energy and 10 Hz of frequency for 2 min, under Ar atmosphere, at 1 Torr of pressure. After this process, the substrate was positioned at a 30 mm distance from the target. At the used gas pressure, the nanoparticles are formed at the plume, which requires a short distance between target and substrate to enlarge the amount of collected material. For technical and simplicity reasons, two types of substrates were used: 1) carbon-coated grids (Ted Pela, inc.) for HR-TEM imaging and 2) Si (001) substrate for crystallographic and magnetic measurements. The deposition rate achieved for all compositions are of 2 mg/h.

Characterization techniques: The targets structural characterization was performed through powder X-ray Diffraction (XRD) using a Rigaku Smartlab Diffractometer with Cu-Kα radiation, 45 kV and 200 mA, at IFIMUP. Data were collected in a Bragg-Brentano geometry at 2θ from 20^0 to 70^0. As for the nanoparticles, the powder was removed from the Si substrate and placed between Kapton tape for the XRD measurements at the ID31 beamline of the European Synchrotron Radiation Facility (ESRF) in Grenoble,

France. The beam spot on the sample was of 2 × 2 μm and the energy of the incident beam was 70 keV (λ = 0.177 Å). The data were collected in the 1.5–8 $Å^{-1}$ Q-range ($Q = 4\pi\sin(\theta)/\lambda$) using a Pilatus3 X CdTe positioned at 1.05 m from the sample. Calibration of the detector was done using CeO_2 NIST SRM 674b material, and azimuthal data integration was performed in pyFAI. For all sample patterns, the crystallographic structures were identified by the *Rietveld* refinements using the *Fullprof* software [25] on the raw data at room temperature. The nanoparticles morphological characterizations were performed through High-Resolution Transmission Electronic Microscopy (HR-TEM) images using a JEOL 2100F–200 kV at LABNANO - CBPF. Magnetic measurements of all samples were performed using a Superconducting Quantum Interference Device (SQUID).

3. Results and discussion

3.1. Structural characterization

The $Gd_5(Si_xGe_{1-x})_4$ nanoparticles were produced by ablating the polished surfaces of the ingots to guarantee the sample stoichiometry, namely, for x = 0, 0.45 and 0.60. The target stoichiometry transfer and the absence of chemical reactants during PLD are the main advantages of this versatile technique [23]. The ablations were performed with an Ar gas flux in a way that the chamber was kept at a constant pressure of 1 Torr. Due to the presence of inert gas, when the high-power laser ablates the target surface, the evaporated atoms randomly collide, forming the NPs in the generated plume. They are then collected by the substrate, positioned at 30 mm from the incident surface [5,26]. Transmission Electronic Microscopy (TEM) and High-resolution TEM (HR-TEM) images were obtained for all compositions. They are shown in Fig. 1(a–f), where it is possible to notice their spherical morphology. For x = 0, depicted in Fig. 1(a), particles with an average size of ~15±0.6 nm and with good crystallinity were obtained, as can be observed from the Selected Area Electron Diffraction (SAED) shown on the inset. As for the NPs with x = 0.45 composition, presented in Fig. 1(b), a particle diameter of ~27±0.9 nm is obtained. The x = 0.60 NPs presented a ~10±0.4 nm average size, as shown in Fig. 1(c). The smaller diameters for x = 0.60 composition, produced under the same conditions as x = 0.45 NPs, can be related to the smaller bulk unit cell volume while the 15 nm for x = 0 is associated with the different wavelength used for the deposition. The first crystalline feature evaluated on these samples was achieved through integrated angular intensity extracted from several SAED images of all samples. The obtained interplanar distances were compared with the three possible crystallographic structures adopted by the $Gd_5(Si,Ge)_4$ family: *i)* Gd_5Ge_4-type with an orthorhombic-II [O(II)] structure, which has the largest unit cell volume, being the x = 0 case; *ii)* $Gd_5Si_2Ge_2$-type with a distorted monoclinic (M), that corresponds to the x = 0.45 composition phase, and; *iii)* Gd_5Si_4-type orthorhombic-I [O(I)] structure that presents the lowest unit cell volume [11]. From the observed SAED peaks, O(I) structure could be indexed for all compositions. Besides, an amplification of one NP for each sample, shown in Fig. 1(d–f), allows a clear observation of the interplanar spacing (d_{hkl}). By measuring the d_{hkl} distances at the NPs high-resolution images, we obtain $d_{hkl} = 2.46$ Å for x = 0 that corresponds to (103) diffraction planes of O(I) phase. While for x = 0.45 and 0.60, a $d_{hkl} \sim 2.70$ Å is obtained that coincides with the (202) diffraction plane of the O(I) phase, confirming the SAED analysis. It is imperative to point out that the associated planes obtained from the d_{hkl} for all compositions are parallel to the *b*-axis. This observation is a strong evidence of the similar growth mechanisms during the pulsed laser ablation that are playing a role in the different $Gd_5(Si,Ge)_4$ nanoparticles. For x = 0.60 nanostructures case, the target crystallographic structure is conserved. Similar to the observed in previous Si-rich compositions of these compounds at the micro/nanoscale [14]. Distinctly, there seems to be a size-induced structural change for x = 0 and 0.45 compositions, which might be related to the atomic coalescence during the nanoparticle nucleation process. In this case, the atoms tend to arrange in a smaller unit cell volume structure, which is the O(I) structure for this family [12]. A change in the atomic structure symmetry for magnetic materials reduced to the micro- and nanoscales is commonly observed [23,27]. However, to the best of our knowledge, there are no reports of a structural transformation for $Gd_5(Si,Ge)_4$ compounds at reduced scales [14,16,18].

Although SAED analysis was used to identify the nanoparticles' crystallographic structures, X-ray diffraction (XRD) measurements are more suitable to clarify the TEM results. The normalized patterns for the targets and NPs with x = 0, 0.45 and 0.60 compositions

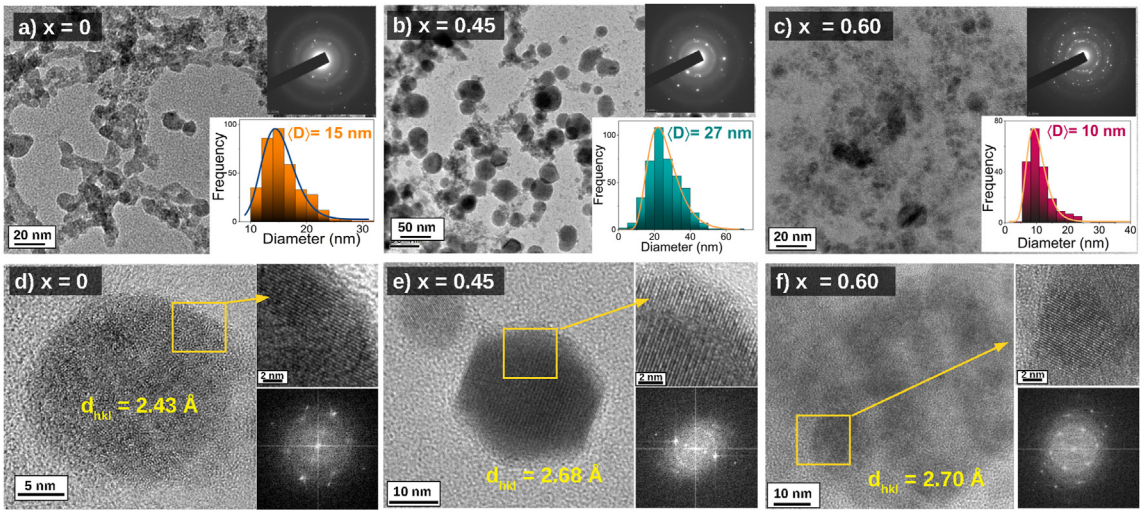

Fig. 1. HR-TEM images and the obtained particle size distribution for **(a)** x = 0, **(b)** x = 0.45 and **(c)** x = 0.60 compositions with their respective selected area electron diffraction (SAED) in the inset revealing the crystalline feature of the collected nanoparticles. From the amplifications in selected particles the interplanar distances were obtained for **(d)** x = 0, **(e)** x = 0.45 and **(f)** x = 0.60.

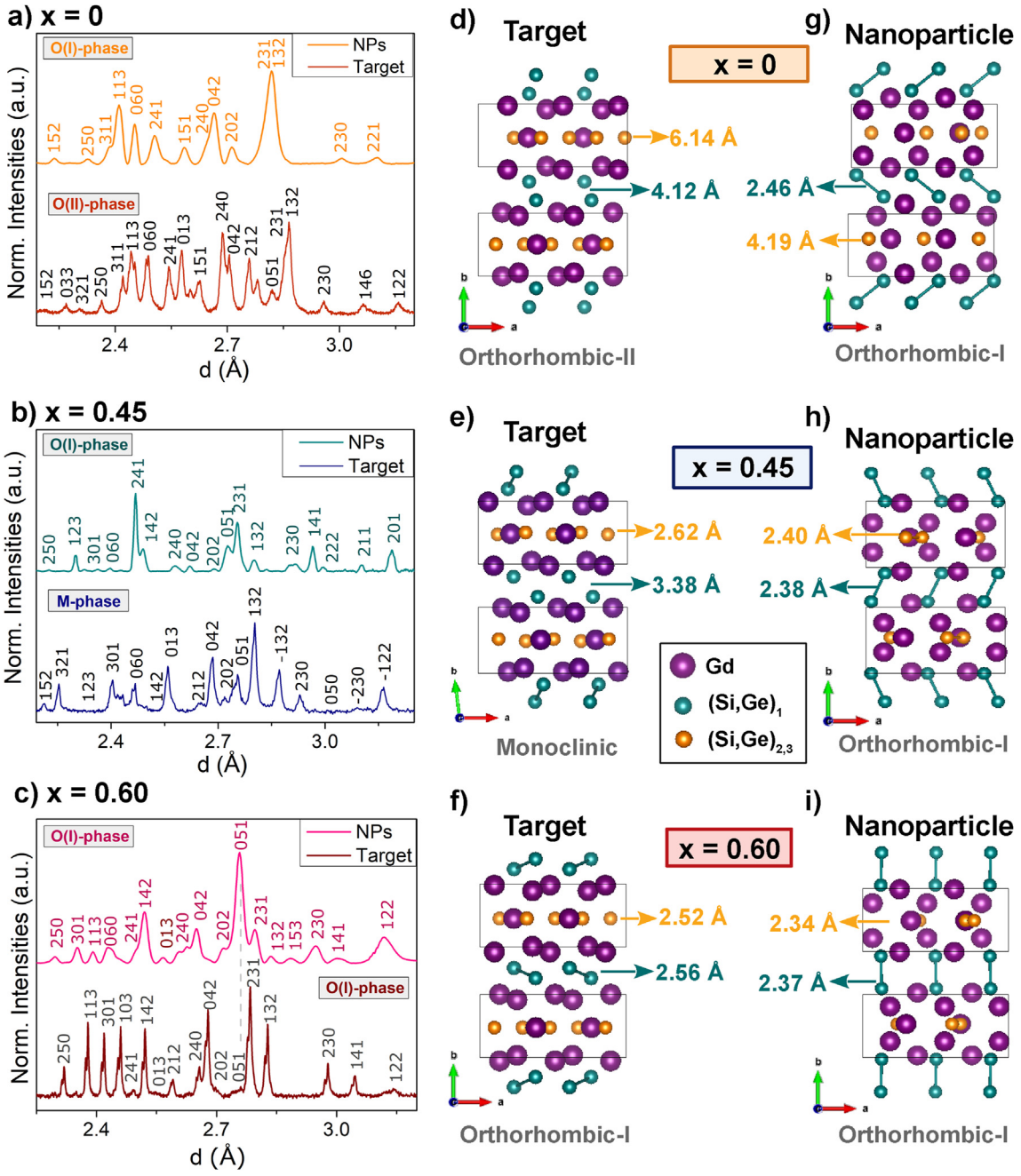

Fig. 2. Comparison between bulk and nanoparticles XRD patterns for **(a)** x = 0, **(b)** x = 0.45 and **(c)** x = 0.60 compositions where it is possible to notice the broadening and shift of the peaks. From *Rietveld* calculations, targets and nanoparticles structures were constructed using the VESTA 3 software [30] for all compositions given from **(d–i)**.

with the depicted Miller indexes of the main peaks given in Fig. 2(a), (b) and (c), respectively. As can be noted, there is a peak shift towards lower d-values in the NPs patterns, revealing a reduction in the lattice parameters, followed by a peak broadening, typical of nanostructures [6,28]. For the x = 0.45 sample, in Fig. 2(b), there is a considerable difference in the diffracted peak positions between NPs and target, consistent with the structural change observed from the TEM images. In contrast, the x = 0.60 NPs pattern presents similar peaks positions when compared to the target diffractogram, as shown in Fig. 2(c). *Rietveld* refinements were performed to confirm these evidences, and the obtained lattice parameters for the targets and NPs are summarized in Table 1. The more considerable lattice parameter reduction observed, going

Table 1
Lattice parameters and the Pseudo-Voigt profile values obtained from Rietveld refinements for targets and NPs of $Gd_5(Si_xGe_{1-x})_4$ obtained from PLD in Ar atmosphere. The orthorhombic-I and II [O(I) and O(II)] structures belong to the Pnma space group and the monoclinic (M) to the $P112_1/a$ space group.

Parameters	x = 0		x = 0.45		x = 0.60	
	Target	NPs	Target	NPs	Target	NPs
	O(II)	O(I)	M	O(I)	O(I)	O(I)
a (Å)	7.674	7.604	7.590	7.509	7.512	7.477
b (Å)	14.80	14.72	14.81	14.76	14.78	14.73
c (Å)	7.770	7.724	7.782	7.782	7.797	7.783
γ (°)	90.00	90.00	93.13	90.00	90.00	90.00
V ($Å^3$)	882.2	864.6	873.4	862.9	865.7	857.5

from the bulk to the nanoparticles, was along the *a*-axis, being of 0.91%, 1.06% and 0.46% for x = 0, 0.45 and 0.60, respectively.This lattice shortening reflects a change in the position of the peaks of diffracted planes parallel to the *a*-axis in Fig. 2(a–c). Most notably, the peaks associated with the (051) and (042) diffraction planes for all compositions shift towards lower d-values. The lattice contraction in metallic materials at reduced scales is a common mechanism. It is related to the surface stress rising from the increase of surface/volume ratio and to the sensitivity to external conditions [6] that can be well described in terms of the capillary stress [29], as discussed below.

From the NPs XRD patterns calculations, the atomic positions were also obtained by *Rietveld* refinements using the bulk structural factors from Ref. [31] as initial values, with the structures presented in the right side of Fig. 2. The calculated patterns and atomic positions are given in Fig. S1 and Table S1, respectively, of the Supporting Information Document (SID). All of these structures are constructed by pseudo-blocks piled along the *b*-axis that are connected by Si(Ge)/Si(Ge) dimers, positioned at the $(Si,Ge)_1$ sites, where the covalent bonds are formed when the $Si(Ge)_1$-$Si(Ge)_1$ distance is below 2.70 Å [31]. For the larger unit cell volume of the O(II) structure, none of these bonds are formed. For the M-phase, due to the structural distortion, only half of these bonds are formed and is one of the main distinction with the O(I) structure that presents all the bonds, as can be observed from Fig. 2(b–f) of the bulk targets. Comparing the x = 0 target [Fig. 2(d)] and the NPs structure of Fig. 2(g), the reduction on the unit cell volume becomes evident from the $Si(Ge)_1$-$Si(Ge)_1$ dimers formation for the NPs. These bonds are not attained at the bulk counterpart due to the crystallization in an O(II) structure. Distinctly, from Fig. 2(e), the x = 0.45 target crystallizes in an M-phase where half of the dimers are formed and, when reduced to 27 nm, all the Si(Ge) are connected, as can be seen in Fig. 2(f). The x = 0.60 composition presents an O(I)-phase in both target and NPs, where the angle between Si(Ge)-Si(Ge) bonds along the *b*-axis give their structural distinction. . For x = 0 and 0.45 nanostructures, the $Ge(Si)_1$-$Ge(Si)_1$ distance is shortened to 2.46 Å and 2.38 Å, respectively, being the responsible for symmetry change from O(II) and M phases to an O(I) structure. In contrast, there is no phase change from the bulk to NP for x = 0.60 composition. However, a reduced $Si(Ge)_1$-$Si(Ge)_1$ distance of 2.37 Å is observed. The shrinkage for this composition is due to the Si(Ge)/Si(Ge) dimers alignment along the *b*-axis, in addition to the lattice parameter reduction aforementioned. The blocks approximation is a direct consequence of the structural packing along the *b*-axis, where an average relative reduction of ~0.40% on the *b* lattice parameter for all compositions of NPs occurs. For the three stoichiometries, there is an improvement in symmetry that might be rising from intrinsic surface pressure during the atoms packing for the nanoparticle formation [3,7,16]. As a matter of fact, these $Si(Ge)_1$-$Si(Ge)_1$ distances are well below those observed for the ones $Gd_5(Si,Ge)_4$ bulk targets, which also contributes to the distinct NPs structural and magnetic features [11,19,31].

3.2. Magnetic and magnetocaloric results

Given the strong relation between crystal structure and magnetic behaviour on the $Gd_5(Si,Ge)_4$ family compounds, magnetization measurements are a powerful tool to confirm and extend the conclusions obtained through XRD and TEM analysis. The normalized magnetization curves acquired using the zero field cooling (ZFC) and field cooling (FC) protocols for the NPs are shown in Fig. 3 together with their respective targets cooling and heatings magnetization curves. It is known that at the Ge-rich region, the system will present a first order magnetic transition (FOMT) with an associated structural change that implies a thermal irreversibility on the magnetization between cooling and heating measurements [11]. In particular, the Gd_5Ge_4 (x = 0) stoichiometry, presents a ferromagnetic (FM) to antiferromagnetic (AFM) transition at low temperature followed by an AFM to paramagnetic (PM) transition. Both magnetic orderings changes can be induced by the applied magnetic field intensity [32]. These transitions become more evident for low intensities of magnetic field and, for this reason, the magnetization measurements for the x = 0 composition were obtained for a 0.001 T of applied field. The curves are shown in Fig. 3(a), where the FM to AFM temperature (T_{FM-AFM}) and Néel (T_N) temperatures are highlighted in the derivative curves on the inset. When the system undergoes to 15 nm of particle size, the bump around 50 K indicates that the Gd_5Ge_4 composition present a spin glass (SG) or a superparamagnetic (SPM) behavior [33]. However, further investigations should be performed to distinguish and conclude the behavior of these nanostructure. In addition, the high temperature transition, that is less attenuated for the nanostructures, might be related with an AFM ordering of the larger particles that are above the critical size for the SPM or SG behavior (see Fig. 1).

As for x = 0.45 target, a thermal irreversibility between 150 and 250 K is observed and corresponds to a FOMT wherein the sample presents an [O(I),FM]→[M,PM] transition [34]. As can be seen on the temperature derivative curves, depicted on the inset of Fig. 3(b), there is a small bump around 290 K for the x = 0.45 target that corresponds to the second order magnetic transition (SOMT) of the O(I)-phase [35]. As for the x = 0.45 particles, a single FM→PM transition is observed at 290 K, which confirms that indeed the system crystallizes in an O(I)-type structure. On the other hand, since there is no change in structure, the x = 0.60 NPs conserves the bulk Curie temperature (T_C) of 310 K. Nonetheless, the irreversibility between the ZFC and FC magnetization curves is larger for the x = 0.60 sample than of x = 0.45 composition which might be related with the narrower particle size distribution for the higher Si content system that increases the particles magnetic anisotropy [28].

For MCE evaluation and order transition investigation, isothermal magnetization measurements were carried out by increasing and decreasing the applied magnetic field intensity up to 5 T for the bulk targets and nanoparticles, shown in Fig. S3 on SID. The x = 0.45 target presents magnetic irreversibility and, when the particle size is reduced to ~ 27 nm, the metamagnetic transition is vanished, indicating a change to a SOMT regime. A similar behaviour is observed for x = 0.60 composition where the disappearance of the irreversibility is followed by a reduction on the magnetization values. These observations are confirmed through the Arrott plot (AP) curves, also shown in Fig. S3, for the nanoparticles. A negative slope is observed for x = 0 and 0.45 target, confirming the FOMT of these systems. As for x = 0.45 and x = 0.60 NPs, there are positive slopes that are attributed to a SOMT, according to the Banerjee's criteria [36]. This change in magnetic transition order is often observed in nanostructured systems, that is due to an increase on the system anisotropy derived from the larger contributions of the surface and/or to an enhanced disorder at the nanoscale [5,28].

The observations from the M(H,T) data is translated on the magnetocaloric effect, once the magnetic transition has already shown to change from a first to a second order one. For the present systems, the magnetic entropy change estimation can be conveniently performed using the discrete integrated Maxwell relation: $\Delta S = \sum_i \delta M_i / \delta T_i \times \delta H$ [36,37] with the results from Fig. S2 on SID. It is worth to pointing out that, since the bulk targets present a FOMT, the entropy change curves cannot be acquired using the Maxwell relation [38]. The calculated magnetic entropy change curves for all

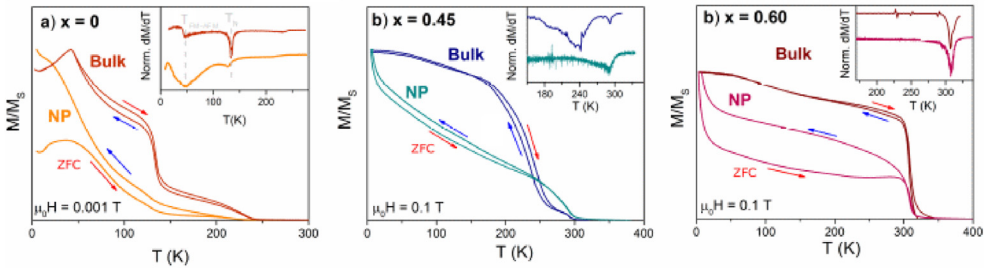

Fig. 3. Temperature dependence on the magnetization curves obtained for **(a)** x = 0, **(b)** x = 0.45 and **(c)** 0.60 compositions as NPs and as targets with their respective temperature derivative curves on the inset.

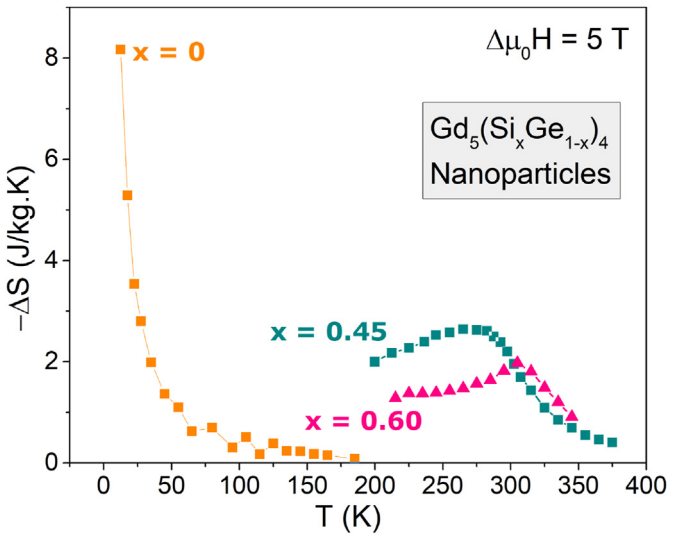

Fig. 4. Temperature dependence of the magnetic entropy change for the $Gd_5(Si_xGe_{1-x})_4$ nanoparticles obtained using the integrated Maxwell relation.

nanostructures are shown in Fig. 4(a). Given the SPM or SG behavior for x = 0 nanoparticle, the curve presents a maximum at the lowest temperature and further decreases, corroborating with the linear decrease of the saturation magnetization with temperature. For x = 0.60 bulk target, there is a reduction on the maximum entropy change and, consequently, on the RCP values, in agreement with previous reports [39]. The nanostructures follow the same compositional trend to the bulk ΔS_{max} values [19]; however, with a larger working range temperature. The temperature span for the MCE doubles from targets to the NPs. Such behavior is also a consequence on the increase of disorder from the reduction of particle size [2,16,28]. In particular, for x = 0.45 composition, the RCP of 289 J/kg is larger than the value obtained by Hadimani et al. for the FOMT granular thin film of $Gd_5Si_{1.3}Ge_{2.7}$ produced by a femtosecond PLD [2,16]. Although a bigger average particle size of ~70 nm was obtained for the thin film, this observation can be related with the absence of hysteresis losses on the nanoparticles produced by nanosecond PLD. Notwithstanding, the relative reduction on the MCE response from the bulk to the nanostructure in the present work averaging 30% is comparable with the 32% observed for $Gd_5Si_{1.3}Ge_{2.7}$ thin film when compared with the system at the macroscale [16].

3.3. Bulk compressibility and intrinsic surface pressure

The $Gd_5(Si,Ge)_4$ family crystallographic and magnetic behaviour is very sensitive to applied pressure, most notably for the Ge-rich compositions. For instance, in situ high pressure synchrotron XRD measurements in a polycrystalline $Gd_5Si_2Ge_2$ sample revealed that

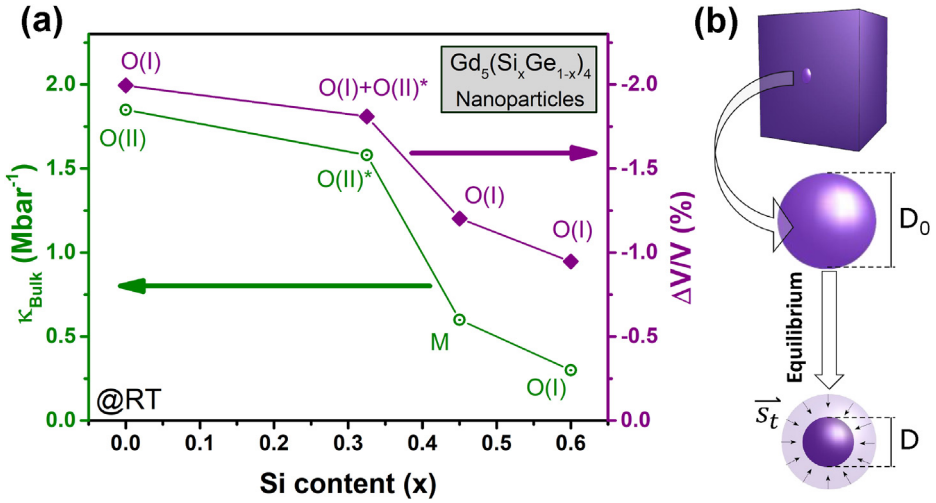

Fig. 5. **(a)** (*right-axis*)Relative unit cell volume change $[(V_{NPs} - V_{bulk})/V_{bulk} = \Delta V/V]$ for $Gd_5(Si_xGe_{1-x})_4$ nanostructures and (*left-axis*)the compressibility values (κ) as a function of Si content (*x*).(*) The x = 0.325 value was obtained from Refs. [16]. As for the κ values, they were extracted from Ref. [16,40]. **(b)** Illustration of the intrinsic surface tension (s_t) rising from the new thermodynamic equilibrium of the nanoparticle with diameter D obtained from the removal of a small piece with D_0 diameter responsible for the unit cell volume reduction.

the system changes from a M to an O(I)-phase when subjected to hydrostatic pressures above 21 kbar [40]. By considering the κ values and using the experimental relative reduction on the unit cell volume, it is possible to estimate the applied pressure on each structural phase of the grains through the thermodynamic relation: $\kappa \sim -(1/V)(\Delta V/\Delta P)$[41]. If we consider the compressibility of 0.60 $Mbar^{-1}$ for x = 0.45 bulk compound from Ref. [40], the corresponding hydrostatic pressure for the observed volume reduction on the nanoparticles should be around 27 kbar. This value is well above the critical 20 kbar for a complete change in structure from a M phase to an O(I) one. In addition, taking into account the pressure dependence of T_C for a close composition (x = 0.50) of dT_C/dP = 6.1 K/kbar [42], the increase of 40 K in T_C corresponds to a hydrostatic pressure of 6.6 kbar, that is above the critical values for a shift on the system transition from a first to a second order one. In this sense, we can conclude that this evidence is a direct consequence of the intrinsic pressure effects from the nanostructure surface, being in agreement with the structural analysis. Nevertheless, this investigation is not required for x = 0.60 composition, once it conserves the structure for the nanoparticles. However, it is worth pointing out that the κ values might be distinct for the nanostructure due to the atomic rearrangement [43].

Given this, the different compositions volumetric compressibility (κ) might be related to their NPs structural characteristics. In this regard, the unit cell volume reduction presented the most relevant changes at the nanoscale. Indeed, for any system presenting crystallinity, the structural parameters are essential to understand their physical properties [6]. In Fig. 5, the relative unit cell volume change $(V_{NP} - V_{bulk})/V_{bulk} = \Delta V/V$, at room temperature, and the κ values for bulk samples obtained from the literature, as a function of Si content, show a linear relationship between these two physical quantities. The values for granular thin film with x = 0.325 composition, from Ref. [3], was included in these results to compare with the effect of ablation the target using a pulse duration of femtosecond. As can be noted, $Gd_5(Si_xGe_{1-x})_4$ compounds with higher Si content present lower κ values, which leads to smaller volumetric variations for the atoms conformation in a nanoparticle. Consequently, it is reasonable to identify the bulk compressibility as the key mechanism controlling the size-induced unit cell reduction.

Most materials at the micro- and nanoscales present a shrinkage of their lattice parameters due to surface stress [7], except for some rare cases, such as hexagonal GaN and SiGe nanoparticles [6]. The particular example of the lattice expansion with decreasing particle size for SiGe nanostructures is attributed to the formation of an oxide shell [44]. Theoretical models considering only elastic deformations for nanostructures have been developed and can predict the lattice contraction of particles with sizes above 1 nm, which is closely related to the bulk features [29]. This relation is because, for solid materials, the surface stress (s_s) is not equal to the surface energy (σ). The first, s_s, is defined as the reversible work per area required to compress a particle while the second arises from intermolecular interactions. The mean stress on the particles' surface is a result of the defects at the boundaries, i.e., at the grains interface [8]. To understand this mechanism, we should consider that only spherical shapes form when a small piece with diameter D_0 is removed from the bulk to form the particles, as shown in Fig. 5(b). In order to achieve a new thermodynamic equilibrium, a surface tension (s_t) emerges contracting its initial radius, leading to a particle with a diameter D, as illustrated in Fig. 5(b). At the equilibrium state, the surface stress due to the internal pressure (p_i) is given as [8]:

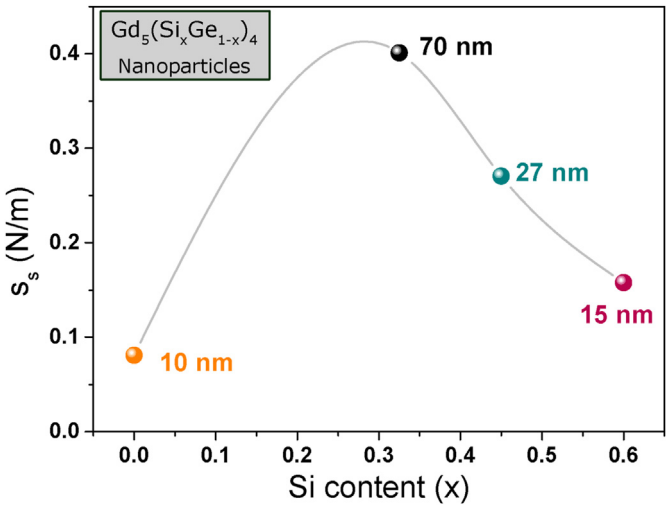

Fig. 6. Surface stress values obtained using equation (2) for the $Gd_5(Si_xGe_{1-x})_4$ nanoparticles produced using femto- and nanosecond PLD techniques.

$$p_i - p_0 = 2s_s/D \tag{1}$$

where p_0 corresponds to the environment pressure. Since $\Delta p = -1/\kappa(\Delta V/V)$, the equation above can be written as follows:

$$\frac{\Delta V}{V} = -2\kappa\frac{s_s}{D} \quad \Rightarrow \quad s_s = -\frac{D}{2\kappa}\frac{\Delta V}{V}. \tag{2}$$

Thus, a linear relationship between the relative unit cell volume variation and the compressibility is obtained, as observed in this study. From Eq. (2) and Fig. 5(a),it was possible to estimate the s_s values as a function of the Si content, shown in Fig. 6, where the relation with the particle size can be observed. The maximum value for x = 0.325 composition [3] is due to the larger particle size for this sample. Conversely, the minimum for x = 0 nanostructures is due to the lower average diameter. It should be pointed out that the obtained s_s values are well below the ones observed for pure metals that range from 1 N/m to 6 N/m [45]. The versatility of the PLD technique allows the optimization of free-particles size, thin film roughness, thickness, composition, etc. The sample features can be controlled by the experimental conditions, such as chamber atmosphere, inert gas flux, target to substrate distance, time of deposition, laser wavelength, pulse duration, energy, frequency and fluency [23]. Thus, by changing the deposition conditions, different particles size can be achieved as shown here and already demonstrated for other systems [26], including Gd-Si-Ge compounds produced through ablation in liquids by varying the laser wavelength and pulse duration [18,20]. Besides, different morphologies are being compared when the particle size is considered: *i)* the ultra-short laser ablation lead to a $Gd_5Si_{1.3}Ge_{2.7}$ (x = 0.325) granular thin film, due to the absence of inert gas [16] and *ii)* the nanosecond laser deposition with Ar atmosphere that resulted in nanoparticles free of substrates. For this reason, it is imperative to produce structures with different diameters by varying the deposition parameters such as the laser energy and inert gas pressure. Here, the presented results demonstrate the possibility to synthesize single-phase nanostructures of $Gd_5(Si,Ge)_4$ with different concentrations, by using nanosecond laser ablation. Furthermore, the origin of the unit cell volume reduction of the achieved nanoparticles produced

through the PLD techniques, using different wavelengths, was demonstrated to be due to a similar growth mechanism closely related to the bulk mechanical features.

4. Conclusions

From the results here presented, we can conclude that nanosecond PLD using 1 Torr of Ar atmosphere is an appropriate approach to obtain $Gd_5(Si_xGe_{1-x})_4$ nanostructures with x = 0, 0.45 and 0.60 with desirable crystallographic properties. The samples' quality is a consequence of the meticulous chamber pressure control where the particle formation occurs from the successive collisions of the ejected materials from the target. As a result, for the x = 0.45 nanostructures, a change in symmetry from an M to an O(I)-type structure is observed. For the x = 0.60 composition, the structural analysis points out the stabilization in a target-like O(I) structure, similar to the corresponding compound. The same crystal structures for this NPs indicates a similar formation mechanism at this narrow Si:Ge ratio by using ns pulsed ablation in Argon atmosphere. For all compositions, a shortening in the Si(Ge)-Si(Ge) dimers are obtained from *Rietveld* refinements. Such findings are translated in a change on the magnetic transition order from a first to a second one for x = 0.45 and 0.60 samples. Distinctly, the x = 0 composition presents a superparamagnetic-like or sping glass behavior that lead to a shortening on the magnetocaloric response. This reduction is a direct result of the unit cell volume shrinkage compared to their bulk counterpart, that was found to be closely related to the bulk compressibility values. Such observations result from intrinsic pressure effects due to the surface/volume ratio that is represented by the surface stress (s_s). Thus, revealing that the growth mechanism of $Gd_5(Si,Ge)_4$ nanostructure through PLD are similar for different laser wavelength and pulse duration.

CRediT authorship contribution statement

V.M. Andrade: Conceptualization, Investigation, Data curation, Formal analysis, Writing - original draft. **J.H. Belo:** Validation, Investigation, Formal analysis, Writing - review & editing. **N.R. Checca:** Methodology, Resources, (TEM images). **A. Rossi:** Resources. **F. Garcia:** Resources, Validation. **B. Almeida:** Resources, Validation, Writing - review & editing. **J.C.G. Tedesco:** Data curation, Validation, Writing - review & editing. **A. Poulain:** Data curation. **A.M. Pereira:** Conceptualization, Validation. **M.S. Reis:** Resources, Supervision, Writing - review & editing. **J.P. Araújo:** Supervision, Funding acquisition, Project administration.

Declaration of competing interest

The authors declare that they have no known competing financial interests or personal relationships that could have appeared to influence the work reported in this paper.

Acknowledgement

This work is funded by FEDER funds through the COMPETE 2020 Programme and National Funds throught FCT - Portuguese Foundation for Science and Technology under the project UID/NAN/50024/2013 and by NECL with the project NORTE-01-0145-FEDER-022096. This work was also supported by the European Union's Horizon −2020 research, innovation program under the Marie Sklodowska-Curie Grant Agreement No. 734801 and by the Fundação de Amparo a Pesquisa do Estado de São Paulo, Brasil (FAPESP) - Project No. 2017/10581-1. The authors would like to thank LABNANO/CBPF for the grants and technical support. We would also like to thank Prof. Kleber R. Pirota for reading the manuscript and contribute with suggestions that were important for the work evaluation. VMA thanks the CNPq for the Grant No. 203180/2014-3. J.H. Belo thanks FCT for the Grant SFRH/BD/88440/2012, the project PTDC/FIS-MAC/31302/2017 and his contract DL57/2016 reference SFRH-BPD-87430/2012. MSR thanks CNPq and FAPERJ for financial support. He belongs to the INCT of Refrigeracão e Termofisica, funding by CNPq by Grant No. 404023/2019-3.

Appendix A. Supplementary data

Supplementary data to this article can be found online at https://doi.org/10.1016/j.jallcom.2020.156384.

References

[1] M.M. Vopson, Theory of giant-caloric effects in multiferroic materials, J. Phys. Appl. Phys. 46 (34) (2013) 345304.
[2] V. Franco, J. Blázquez, J. Ipus, J. Law, L. Moreno-Ramírez, A. Conde, Magnetocaloric effect: from materials research to refrigeration devices, Prog. Mater. Sci. 93 (2018) 112−232.
[3] J.H. Belo, A.L. Pires, I.T. Gomes, V. Andrade, J.B. Sousa, R.L. Hadimani, D.C. Jiles, Y. Ren, X. Zhang, J.P. Araújo, Giant negative thermal expansion at the nanoscale in the multifunctional material $Gd_5(Si,Ge)_4$, Phys. Rev. B 100 (13) (2019) 134303.
[4] V. Andrade, A. Amirov, D. Yusupov, B. Pimentel, N. Barroca, A. Pires, J. Belo, A. Pereira, M. Valente, J. Araújo, Multicaloric effect in a multiferroic composite of $Gd_5(Si,Ge)_4$ microparticles embedded into a ferroelectric PVDF matrix, Sci. Rep. 9 (1) (2019) 1−10.
[5] D. Vollath, Nanoparticles-Nanocomposites-Nanomaterials: an Introduction for Beginners, John Wiley & Sons, 2013.
[6] P.M. Diehm, P. Ágoston, K. Albe, Size-dependent lattice expansion in nanoparticles: reality or anomaly? ChemPhysChem 13 (10) (2012) 2443−2454.
[7] J. Vermaak, C. Mays, D. Kuhlmann-Wilsdorf, On surface stress and surface tension: I. theoretical considerations, Surf. Sci. 12 (2) (1968) 128−133.
[8] J. Weissmüller, J. Cahn, Mean stresses in microstructures due to interface stresses: a generalization of a capillary equation for solids, Acta Mater. 45 (5) (1997) 1899−1906.
[9] T. Gottschall, A. Gràcia-Condal, M. Fries, A. Taubel, L. Pfeuffer, L. Mañosa, A. Planes, K.P. Skokov, O. Gutfleisch, A multicaloric cooling cycle that exploits thermal hysteresis, Nat. Mater. 17 (10) (2018) 929.
[10] K. Gschneidner, V. Pecharsky, A. Pecharsky, V. Ivtchenko, E. Levin, The Nonpareil $R_5(Si_xGe_{1-x})_4$ Phases.
[11] V. Pecharsky, K. Gschneidner Jr., Phase relationships and crystallography in the pseudobinary system Gd_5si_4 - Gd_5Ge_4, J. Alloys Compd. 260 (1−2) (1997) 98−106.
[12] J.H. Belo, A.L. Pires, J.P. Araújo, A.M. Pereira, Magnetocaloric materials: from micro-to nanoscale, J. Mater. Res. (2018) 1−24.
[13] S.N. Sambandam, B. Bethala, D.K. Sood, S. Bhansali, Evaluation of silicon nitride as a diffusion barrier for Gd-Si-Ge films on silicon, Surf. Coating. Technol. 200 (5) (2005) 1335−1340.
[14] R. Hadimani, S. Gupta, S. Harstad, V. Pecharsky, D. Jiles, Investigation of room temperature ferromagnetic nanoparticles of Gd_5Si_4, IEEE Trans. Magn. 51 (11) (2015) 1−4.
[15] R.L. Hadimani, I. Nlebedim, Y. Melikhov, D.C. Jiles, Growth and characterisation of $Gd_5(Si_xGe_{1-x})_4$ thin film, J. Appl. Phys. 113 (17) (2013) 17A935.
[16] R.L. Hadimani, J.H. Silva, A.M. Pereira, D.L. Schlagel, T.A. Lograsso, Y. Ren, X. Zhang, D.C. Jiles, J.P. Araújo, $Gd_5(Si,Ge)_4$ thin film displaying large magnetocaloric and strain effects due to magnetostructural transition, Appl. Phys. Lett. 106 (3) (2015), 032402.
[17] P. Lorazo, L.J. Lewis, M. Meunier, Thermodynamic pathways to melting, ablation, and solidification in absorbing solids under pulsed laser irradiation, Phys. Rev. B 73 (13) (2006) 134108.
[18] N. Tarasenka, V. Pankov, A. Butsen, N. Tarasenko, Laser assisted synthesis, structural and magnetic characterization of gadolinium germano-silicide nanoparticles in liquid, J. Nanosci. Nanotechnol. 16 (7) (2016) 7451−7460.
[19] V.K. Pecharsky, K.A. Gschneidner Jr., $Gd_5(Si_xGe_{1-x})$ 4: an extremum material, Adv. Mater. 13 (9) (2001) 683−686.
[20] N. Tarasenka, V. Kiris, E. Stankevičius, N. Tarasenko, V. Pankov, F. Krčma, P. Gečys, G. Račiukaitis, Laser irradiation of Gd-Si and Gd-Si-Ge colloid mixtures for the fabrication of compound nanoparticles, ChemPhysChem 19 (23) (2018) 3247−3256.
[21] D. Tan, S. Zhou, J. Qiu, N. Khusro, Preparation of functional nanomaterials with femtosecond laser ablation in solution, J. Photochem. Photobiol. C Photochem. Rev. 17 (2013) 50−68.
[22] K.-H. Leitz, B. Redlingshöfer, Y. Reg, A. Otto, M. Schmidt, Metal ablation with short and ultrashort laser pulses, Physics Procedia 12 (2011) 230−238.
[23] H.-U. Krebs, Pulsed Laser Deposition of Metals, Pulsed Laser Deposition of Thin Films: Applications-Led Growth of Functional Materials, 2007, p. 363.
[24] I. Horn, M. Guillong, D. Günther, Wavelength dependant ablation rates for metals and silicate glasses using homogenized laser beam

profiles—implications for LA-ICP-MS, Appl. Surf. Sci. 182 (1–2) (2001) 91–102.
[25] J. Rodríguez-Carvajal, Recent advances in magnetic structure determination by neutron powder diffraction, Phys. B Condens. Matter 192 (1) (1993) 55–69.
[26] N. Checca, R. Caraballo-Vivas, R. Torrão, A. Rossi, M. Reis, Phase composition and growth mechanisms of half-metal heusler alloy produced by pulsed laser deposition: from core-shell nanoparticles to amorphous randomic clusters, Mater. Chem. Phys. 196 (2017) 103–108.
[27] A. López-Ortega, E. Lottini, C.d.J. Fernandez, C. Sangregorio, Exploring the magnetic properties of cobalt-ferrite nanoparticles for the development of a rare-earth-free permanent magnet, Chem. Mater. 27 (11) (2015) 4048–4056.
[28] V.M. Andrade, R.C. Vivas, S.S. Pedro, J.C.G. Tedesco, A.L. Rossi, A.A. Coelho, D.L. Rocco, M.S. Reis, Magnetic and magnetocaloric properties of $La_{0.6}Ca_{0.4}MnO_3$ tunable by particle size and dimensionality, Acta Mater. 102 (2016) 49–55.
[29] Z. Huang, P. Thomson, S. Di, Lattice contractions of a nanoparticle due to the surface tension: a model of elasticity, J. Phys. Chem. Solid. 68 (4) (2007) 530–535.
[30] K. Momma, F. Izumi, Vesta 3 for three-dimensional visualization of crystal, volumetric and morphology data, J. Appl. Crystallogr. 44 (6) (2011) 1272–1276.
[31] S. Misra, G.J. Miller, On the distribution of tetrelide atoms (Si,Ge) in $Gd_5(Si_xGe_{1-x})_4$, J. Solid State Chem. 179 (8) (2006) 2290–2297.
[32] C. Magen, Z. Arnold, L. Morellon, Y. Skorokhod, P. Algarabel, M. Ibarra, J. Kamarad, Pressure-induced three-dimensional ferromagnetic correlations in the giant magnetocaloric compound Gd_5Ge_5, Phys. Rev. Lett. 91 (20) (2003) 207202.
[33] M. Bandyopadhyay, S. Dattagupta, Memory in nanomagnetic systems: superparamagnetism versus spin-glass behavior, Phys. Rev. B 74 (21) (2006) 214410.
[34] L. Morellon, P. Algarabel, M. Ibarra, J. Blasco, B. Garcia-Landa, Z. Arnold, F. Albertini, Magnetic-field-induced structural phase transition in $Gd_5(S_{1.8}Ge_{2.2})$, Phys. Rev. B 58 (22) (1998) R14721.
[35] R. Hadimani, Y. Melikhov, D. Schlagel, T. Lograsso, D. Jiles, Study of the second-order “hidden” phase transition of the monoclinic phase in the mixed phase region of $Gd5(Si,Ge)_4$, IEEE Trans. Magn. 48 (11) (2012) 4070–4073.
[36] M. Reis, Fundamentals of Magnetism, Elsevier, 2013.
[37] V. Andrade, S. Pedro, R.C. Vivas, D. Rocco, M. Reis, A. Campos, A.d.A. Coelho, M. Escote, A. Zenatti, A. Rossi, Magnetocaloric functional properties of $Sm_{0.6}Sr_{0.4}MnO_3$ manganite due to advanced nanostructured morphology, Mater. Chem. Phys. 172 (2016) 20–25.
[38] J. Amaral, N. Silva, V. Amaral, Estimating spontaneous magnetization from a mean field analysis of the magnetic entropy change, J. Magn. Magn Mater. 322 (9–12) (2010) 1569–1571.
[39] F.C. i Fernàndez, Magnetocaloric Effect in $Gd_5(Si_xGe_{1-x})_4$ alloys, Ph.D. Thesis, Universitat de Barcelona, 2003. December.
[40] Y. Mudryk, Y. Lee, T. Vogt, K. Gschneidner Jr., V. Pecharsky, Polymorphism of $Gd_5Si_2Ge_2$: the equivalence of temperature, magnetic field, and chemical and hydrostatic pressures, Phys. Rev. B 71 (17) (2005) 174104.
[41] J. Belo, A. Pereira, J. Ventura, G. Oliveira, J. Araújo, P. Tavares, L. Fernandes, P. Algarabel, C. Magen, L. Morellon, Phase control studies in $Gd_5Si_2Ge_2$ giant magnetocaloric compound, J. Alloys Compd. 529 (2012) 89–95.
[42] A.M.G. Carvalho, C.S. Alves, A. de Campos, A.A. Coelho, S. Gama, F.C. Gandra, P.J. von Ranke, N.A. Oliveira, The magnetic and magnetocaloric properties of $Gd_5Ge_2Si_2$ compound under hydrostatic pressure, J. Appl. Phys. 97 (10) (2005) 10M320.
[43] B. Gilbert, H. Zhang, B. Chen, M. Kunz, F. Huang, J. Banfield, Compressibility of zinc sulfide nanoparticles, Phys. Rev. B 74 (11) (2006) 115405.
[44] D. Shreiber, W. Jesser, Size dependence of lattice parameter for Si_xge_{1-x} nanoparticles, Surf. Sci. 600 (19) (2006) 4584–4590.
[45] R. Lamber, S. Wetjen, N.I. Jaeger, Size dependence of the lattice parameter of small palladium particles, Phys. Rev. B 51 (16) (1995) 10968.